nature geoscience

Article

https://doi.org/10.1038/s41561-024-01593-0

Multi-month forecasts of marine heatwaves and ocean acidification extremes

Received: 19 January 2024

Accepted: 22 October 2024

Published online: 21 November 2024

Check for updates

Samuel C. Mogen[1] ✉, Nicole S. Lovenduski[1], Stephen G. Yeager[2], Antonietta Capotondi[3,4], Michael G. Jacox[4,5], Stephen Bograd[5], Emanuele Di Lorenzo[6], Elliot L. Hazen[5], Mercedes Pozo Buil[5,7], Who Kim[2] & Nan Rosenbloom[2]

Marine heatwaves and ocean acidification extreme events are periods during which temperature and acidification reach statistically extreme levels (90th percentile), relative to normal variability, potentially endangering ecosystems. As the threats from marine heatwaves and ocean acidification extreme events grow with climate change, there is need for skilful predictions of events months to years in advance. Previous work has demonstrated that climate models can predict marine heatwaves up to 12 months in advance in key regions, but forecasting of ocean acidification extreme events has been difficult due to the complexity of the processes leading to extremes and sparse observations. Here we use the Community Earth System Model Seasonal-to-Multiyear Large Ensemble to make predictions of marine heatwaves and two forms of ocean acidification extreme events, as defined by anomalies in hydrogen ion concentration and aragonite saturation state. We show that the ensemble skilfully predicts marine heatwaves and ocean acidification extreme events as defined by aragonite saturation state up to 1 year in advance. Predictive skill for ocean acidification extremes as defined by hydrogen ion concentration is lower, probably reflecting mismatch between model and observed state. Skill is highest in the eastern Pacific, reflecting the predictable contribution of El Niño/Southern Oscillation to regional variability. A forecast generated in late 2023 during the 2023–2024 El Niño event finds high likelihood for widespread marine heatwaves and ocean acidification extreme events in 2024.

Alongside long-term alterations to the marine system associated with anthropogenic climate change[1–4], there is increasing concern for short-term extreme events that can have dramatic impacts on marine ecosystems[5–7]. Accurate forecasts of extreme events have the potential to alter management practices in advance to plan for, if not mitigate, impacts on marine ecosystems[8]. Marine heatwaves (MHWs), extremes in ocean temperature, are relatively well studied and driven by a variety of atmospheric and oceanic dynamical processes[9–14]. MHWs can have profound impacts on marine organisms and ecosystems. They have been shown to alter primary productivity[15], stress keystone species[16] and induce dramatic species redistribution[17]. They can also impact regional biodiversity[18] and biogeochemistry[5] in the surface and subsurface ocean[19].

By contrast, ocean acidification extremes (OAXs) are relatively understudied, due in part to a historically limited observational record, although recent literature discusses the development, location and impacts of OAXs[20–25]. Previous work has focused on two forms of OAX: high hydrogen ion concentration ($[H^+]$) and low saturation state of seawater in relation to the carbonate mineral aragonite (Ω_a). Ω_a is the degree of saturation of seawater with respect to the mineral

A full list of affiliations appears at the end of the paper. ✉e-mail: samuel.mogen@colorado.edu

https://doi.org/10.1038/s41561-024-01593-0

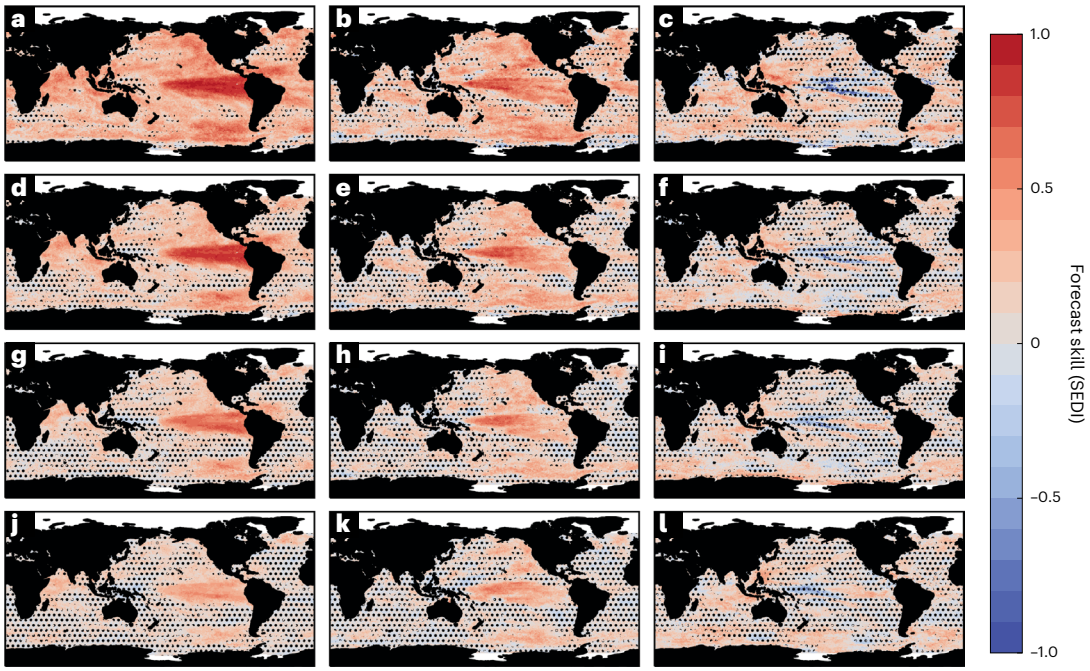

Fig. 1 | Forecast skill for MHW, OAX (Ω_a), and OAX ([H$^+$]). a–l, Forecast skill (SEDI) for MHW (**a**, **d**, **g** and **j**), OAX (Ω_a) (**b**, **e**, **h** and **k**), and OAX ([H$^+$]) (**c**, **f**, **i** and **l**) for 20 ensemble members from CESM SMYLE at 1.5 (**a**–**c**), 3.5 (**d**–**f**), 6.5 (**g**–**i**) and 10.5 (**j**–**l**) months lead time. Skill scores range from −1 to 1, with skill close to −1 being unskilful, skill of 0 being no better than random forecasts and skill of 1 being perfect skill. Dots indicate where skill is not significantly better than random forecasts at the 95% confidence interval.

aragonite[26]; high values of Ω_a support aragonite shell maintenance, while low values are associated with aragonite shell dissolution. Calcifying organisms are negatively impacted during periods characterized by anomalously low Ω_a (refs. 27–29). Both [H$^+$] and Ω_a are important measures of acidification with differing impacts on, and responses from, marine organisms[23,30,31]. For example, pteropods, a type of aragonitic zooplankton, respond to variations in both Ω_a (impacting shell growth, dissolution and survival[31–33]) and [H$^+$] (impacting embryonic development[34]). While extremes in [H$^+$] and Ω_a may co-occur[24], they are commonly driven by different physical processes[23]. The drivers of extremes in [H$^+$] vary regionally. Subtropical [H$^+$] extremes are generally driven by increased temperatures while advection of carbon-rich water is the primary control in the tropics and mid to high latitudes (where vertical mixing also plays a role). Extremes in Ω_a are globally driven by enhanced vertical mixing of carbon-rich subsurface water[23]. As such, while the occurrence of MHWs may be regionally tied to OAXs (for example, co-occurring [H$^+$] extremes and MHWs in the subtropics[23]), OAXs are also driven by enhanced vertical mixing and advection (which are often suppressed during MHWs).

Initialized Earth system model forecasts simulate the evolution of the coupled carbon–climate system from a baseline state of historical model reconstruction and have demonstrated skilful seasonal to interannual forecasts of marine stressors, including temperature[35,36] and ocean acidification[36,37]. Reference 8 skilfully forecast surface MHWs up to 1 year in advance using the physics-only North American Multi-model Ensemble, a collection of global climate model forecasts. They find that MHW forecast skill depends on the El Niño/Southern Oscillation (ENSO) state. Similarly, ref. 38 used the CMCC (Euro-Mediterranean Center on Climate Change) Seasonal Prediction System version 3.5 (CMCC-SPS3.5) and found high potential for predicting subsurface heatwaves. No previous work has examined the forecast skill and predictability of OAXs.

In this Article, we use the Community Earth System Model (CESM) Seasonal to Multiyear Large Ensemble (SMYLE) to forecast surface ocean MHWs and OAXs (both [H$^+$] and Ω_a) events. CESM SMYLE generates forecasts of the short-term evolution of the Earth system, initialized from a reconstruction of the historical ocean (SMYLE Forced Ocean–Sea Ice (FOSI))[39]. CESM SMYLE has previously demonstrated high forecast skill for biogeochemical (dissolved oxygen, dissolved inorganic carbon) and physical (temperature) tracers in both the surface and subsurface ocean up to a year following initialization[36,39]. CESM SMYLE has also demonstrated high forecast skill for ENSO anomalies, performing similarly to other seasonal forecast systems[39]. Here, model forecasts are validated with observations over the historical period for extreme events in the surface ocean at the 90th percentile threshold. We find regions of notably high forecast skill over the historical record, including in the eastern tropical and northeast Pacific. We use forecasts generated in late 2023 to assess the likelihood of global MHWs and OAXs in the coming year, finding high likelihood for widespread marine extremes throughout 2024.

Skilful forecasts of marine extreme events

CESM SMYLE skilfully forecasts surface MHWs and OAXs (Ω_a) up to a year in advance regionally, while OAX ([H$^+$]) has generally lower forecast skill (Fig. 1). Using the Symmetric Extremal Dependence Index (SEDI; Methods), we find significant skill relative to 1,000 random forecasts at the 95% confidence interval 1.5 months after initialization for MHWs and OAXs (Ω_a) globally, with lower global skill in OAX ([H$^+$]) (Fig. 1, row 1). Skill degrades with forecast lead time, although MHW forecasts remain significantly skilful in the eastern tropical, northeastern, and southeastern Pacific up to 10.5 months after initialization (Fig. 1). Similarly, OAX (Ω_a) skill remains significant in the central tropical, northeast, and south Pacific for up to 10.5 months; with skill noticeably higher in the northeast Pacific than for MHW forecasts. By contrast, OAX ([H$^+$]) skill is globally lower 1.5 months after initialization and further degrades with forecast lead time, with limited significant forecast skill in the eastern tropical Pacific at all lead times (Fig. 1, third column).

Two other metrics of model skill—forecast accuracy and Brier Skill Score—support results from SEDI (Extended Data Fig. 1 and Methods), with the tropical Pacific exhibiting high skill for MHW and OAX (Ω_a)

https://doi.org/10.1038/s41561-024-01593-0

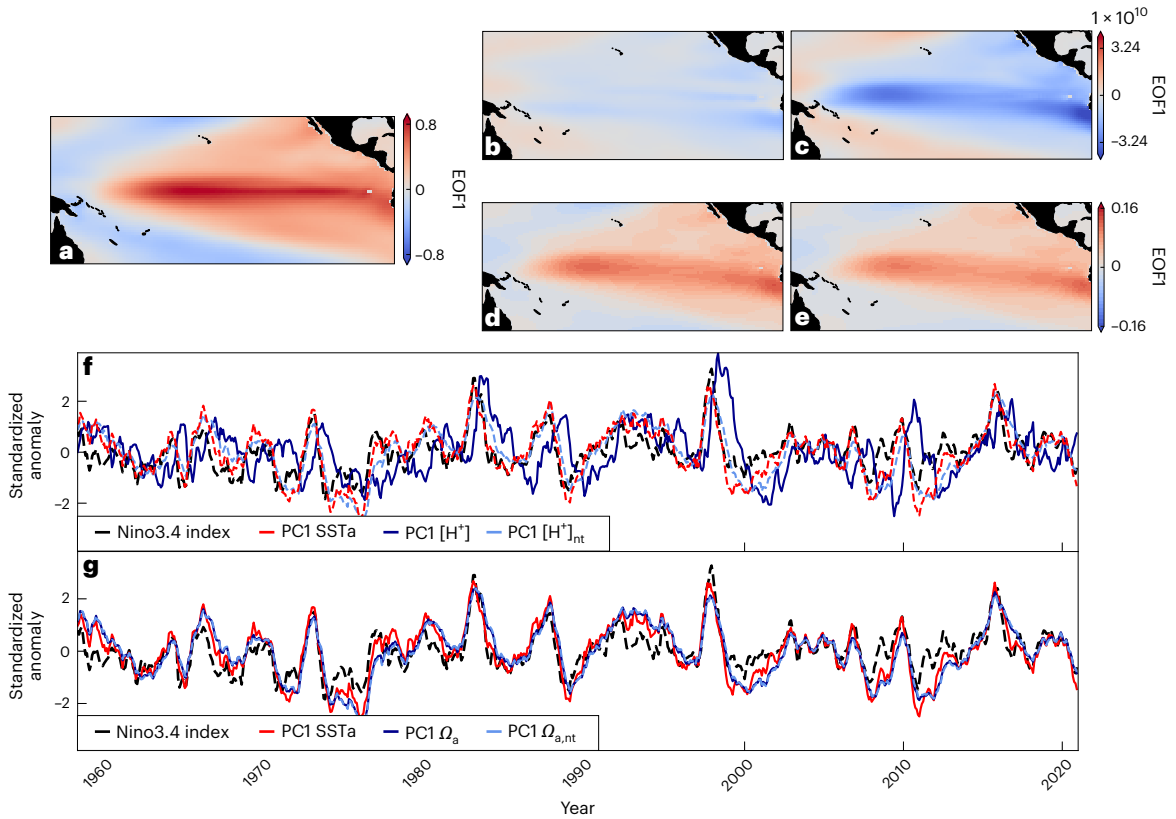

Fig. 2 | Dominant modes of tropical Pacific variability in SMYLE FOSI from principal component analysis. a–e, The first EOF (EOF1) regressed onto anomalies is displayed for SST (**a**), $[H^+]$ (**b**), $[H^+]_{nt}$ (**c**), Ω_a (**d**) and $\Omega_{a,nt}$ (**e**) variability in the tropical Pacific region. **f**, The first principal component (PC1) of tropical Pacific SST (red), $[H^+]$ (blue) and $[H^+]_{nt}$ (blue dashed) variability and the Niño3.4 index (black dashed). **g**, As in **f** but for Ω_a (blue) and $\Omega_{a,nt}$ (blue dashed).

and generally lower skill for OAX ($[H^+]$). CESM SMYLE also successfully estimates the typical frequency and intensity for historical MHWs and OAXs, but consistently overestimates the duration of these extreme events at a given location (Extended Data Fig. 2).

MHW forecast skill is comparable to that reported by ref. 8, with similar regions (for example, the eastern tropical Pacific) demonstrating significant and long-lasting skill for MHWs. OAX (Ω_a) skill mirrors that of MHW, while OAX ($[H^+]$) shows distinct patterns. Regions shown to be skilful in CESM SMYLE correspond to those that exhibit high correlation in the temporal variability and occurrence of extremes between SMYLE FOSI, the historical reconstruction used in initializing CESM SMYLE, and observations, including the tropical and northeast Pacific (Extended Data Fig. 3). MHW and OAX (Ω_a) forecasts are thus expected to demonstrate higher skill because CESM2 can successfully recreate these events in the tropical and northeast Pacific in the FOSI state estimate.

ENSO state enhances forecast skill

What is driving high and long-lasting skill in MHW and OAX (Ω_a) and low skill in OAX ($[H^+]$)? As noted in previous work, ENSO imprints on the seasonal to multiyear forecast skill for physical and biogeochemical variability, and has been linked to MHWs in regions including the tropical and northeast Pacific[8,36,40], although the ENSO influence in the Northeast Pacific may be mediated by North Pacific decadal variability[41–43]. Further, the highest correlations in the historical occurrence of variability and extreme events between the SMYLE FOSI model reconstruction and observations (Extended Data Fig. 3), as well as the highest extreme event forecast skill (Fig. 1), occur in regions associated with ENSO-based variability in the tropical Pacific. ENSO is thus probably an important driver of forecast skill in the tropical and Northeast Pacific.

We examine the dominant modes of variability in our variables of interest in the tropical Pacific (region bounded by latitude 30° S–30° N and longitude 140° E–280° E) to illustrate the relationship between physics and biogeochemistry, and their linkages to ENSO, using empirical orthogonal function (EOF) analysis of SMYLE FOSI (Fig. 2 and Methods). The dominant modes of variability in tropical Pacific sea surface temperature (SST) and Ω_a anomalies are characterized by a similar spatial pattern reminiscent of ENSO (Fig. 2a,d). Indeed, the first principal components of SST and Ω_a anomalies are highly correlated with the Niño3.4 index ($r_{SST} = 0.84, P < 0.05$; $r_{\Omega_a} = 0.75, P < 0.05$). Meanwhile, the dominant mode of variability in tropical Pacific $[H^+]$ anomalies exhibits a different spatial pattern, and its first principal component has a much lower correlation with the Niño3.4 index ($r_{[H^+]} = 0.07$, $P > 0.05$) (Fig. 2b,f), although we note a higher correlation when lagged by 9 months ($r_{[H+],9monthlag} = 0.65, P > 0.05$).

MHWs induce direct changes in $[H^+]$ by altering the carbonate chemistry equilibrium constants[23,44,45]. When MHWs are driven by physical ocean processes (for example, stratification of the upper ocean or reduced upwelling), the circulation of inorganic carbon is also affected, which can have an indirect influence on both $[H^+]$ and Ω_a (refs. 23,45). We demonstrate that circulation-driven $[H^+]$ variability is closely tied to Niño3.4 by performing EOF analysis on tropical Pacific nonthermal $[H^+]$ ($[H^+]_{nt}$), where the direct effects of temperature on the equilibrium constants have been removed from $[H^+]$. The leading EOF of tropical Pacific $[H^+]_{nt}$ variability has a spatial pattern similar to that of Ω_a (Fig. 2c,d), with the first principal component more highly correlated with Niño3.4 ($r_{[H+]_{nt}} = 0.71, P < 0.05$) than $[H^+]$. By contrast, Ω_a variability is unaffected by temperature variability, as the first principal component of both Ω_a and $\Omega_{a,nt}$ are highly correlated with the Niño3.4 index ($r_{\Omega_{a,nt}} = 0.73, P < 0.05$, $r_{\Omega_a} = 0.75, P < 0.05$). While we do not attempt to forecast $[H^+]_{nt}$ using CESM SMYLE (a forecast of $[H^+]_{nt}$ would offer little practical information), we would nevertheless expect higher SEDI skill score values. As the primary modes of tropical

https://doi.org/10.1038/s41561-024-01593-0

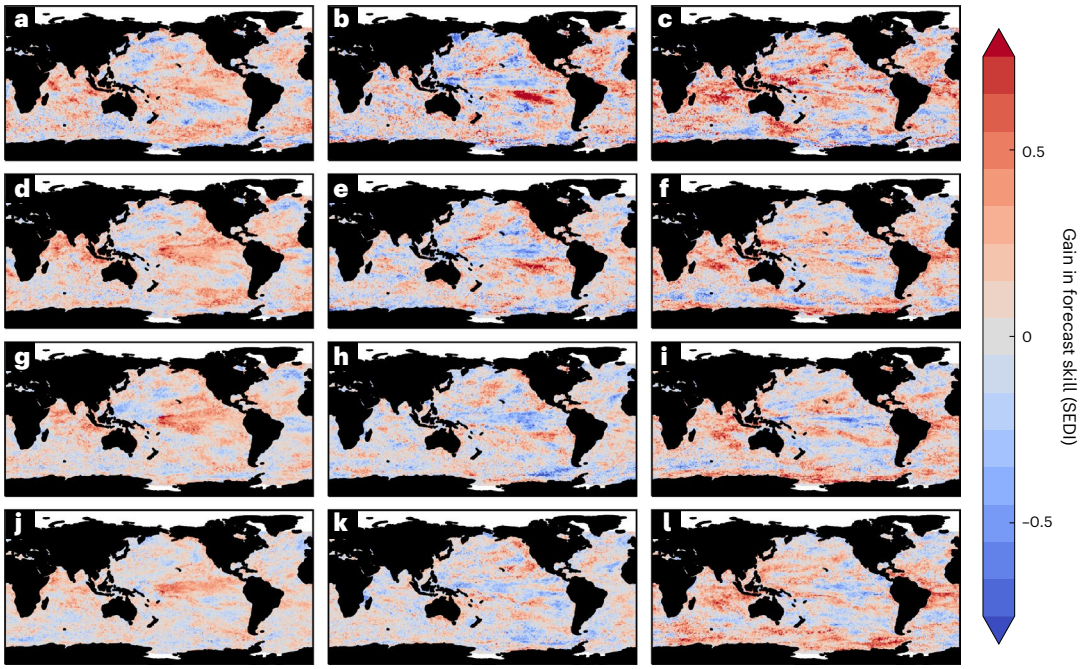

Fig. 3 | Gain in SEDI forecast skill from forecasts initialized during ENSO events (El Niño or La Niña) relative to forecasts initialized during neutral ENSO conditions. a–l, Gain in skill is displayed for MHWs (**a**, **c**, **g** and **j**), OAX (Ω_a) (**b**, **e**, **h** and **k**) and OAX ([H$^+$]) (**c**, **f**, **i** and **l**) at 1.5 months lead time (**a**–**c**), 3.5 months lead time (**d**–**f**), 6.5 months lead time (**g**–**i**) and 10.5 months lead time (**j**–**l**). Positive values indicate a gain in forecast skill during ENSO conditions, while negative values indicate a gain in forecast skill during neutral conditions.

Pacific variability of SST, Ω_a, $\Omega_{a,nt}$ and $[H^+]_{nt}$ exhibit strong spatial and temporal correlations with ENSO, we expect forecasts made during ENSO events (both El Niño and La Niña) to be more skilful than those made during neutral conditions. We thus systematically determine the differences in skill when the model is initialized during (positive or negative) ENSO or neutral ENSO conditions.

In many regions, there is a gain in skill when an extreme event forecast is generated during ENSO (El Niño or La Niña) conditions, demonstrating the role of ENSO in engendering skilful forecasts of MHW and OAX as in ref. 8 (Fig. 3 and Methods). MHWs show a gain in skill during ENSO conditions for the first year of model integration, most notably in the tropical Pacific. Gain in MHW forecast skill increases for up 10.5 lead months after initialization, implying that forecast initialization during an ENSO event drives long-lasting gains in skill. OAX (Ω_a) also demonstrates some regional gains in skill when initialized during an ENSO event, particularly in the eastern tropical Pacific, California Current and Gulf of Alaska regions. Similarly, OAX ([H$^+$]) demonstrate regional gains in skill during ENSO events. Surprisingly, the gain in skill for OAX ([H$^+$]) manifests more broadly than that of OAX (Ω_a) despite the latter being consistently more skilful at all lead times (per Fig. 1) and the weaker relationship between modelled [H$^+$] variability and ENSO (Fig. 2). Although OAX ([H$^+$]) does exhibit a stronger gain in skill, absolute skill scores are still relatively low compared with OAX (Ω_a) (as reflected in the magnitude of skill in Fig. 1).

Our analysis shows that the two indicators of OAXs are not forecast equally well, and they do not respond identically to ENSO variability, with OAXs defined by extremes in Ω_a exhibiting higher forecast skill than those defined using [H$^+$]. Both indicators of OAXs are important stressors for marine ecosystems; why can we only predict one? OAX ([H$^+$]) forecast skill is low due to the model's inability to capture observed [H$^+$] variability. Extended Data Fig. 4 demonstrates high model predictability, illustrating that forecasts of [H$^+$] extremes have the potential to be skilful across the global ocean (predictability is determined by verifying CESM SMYLE forecasts against SMYLE FOSI). However, this potential predictability is not realized as forecast skill. As such, improvements in the model representation of [H$^+$] variability to better match observed variability could increase the forecast skill of OAX ([H$^+$]). High skill for OAX (Ω_a), by contrast, corresponds to low model bias in Ω_a variability (Extended Data Fig. 3). Changes in Ω_a during extreme events are driven primarily by variations in $[CO_3]^{2-}$, which in turn derive primarily from variability in dissolved inorganic carbon (DIC; Extended Data Fig. 5). During OAX (Ω_a), the DIC circulation tendency affects change in surface ocean DIC, with air–sea CO_2 flux and biology playing less important roles in the anomalous DIC budget. These results inform future studies on the utility of OAX forecasts for marine managers.

Forecasts of widespread marine extremes in 2024

Forecasts generated in November of 2023 predict widespread MHW and OAX (Ω_a) events in 2024 (Fig. 4). As these forecasts were generated during an El Niño event, we expect forecasts of MHW and OAX (Ω_a) to have high skill in regions with ENSO-related predictability (as in Fig. 1). The 2023–2024 ENSO event represents an excellent test bed and application for an initialized Earth system model to forecast marine extreme events, as we can expect a forecast generated in late 2023 to be skilful in some regions up to a year in advance. The 2023–2024 El Niño in CESM SMYLE is forecast to peak in January 2024 before declining by June 2024 (Fig. 4a). This forecast is consistent with a suite of available dynamical ENSO forecasts generated in November 2023, indicating a peak in El Niño centred in January 2024 with decline in conditions by June 2024, and is further consistent with the evolution of the Niño3.4 index derived from observations through March 2024[46,47].

CESM SMYLE forecasts indicate that MHWs are highly likely in the eastern Pacific in early 2024, before becoming globally widespread (Fig. 4b,d,f,h,j). In these forecasts, we find a strong signal of ENSO-driven MHWs (present at the month of initialization) in the eastern tropical Pacific that spreads throughout the tropical Pacific through June 2024. The ENSO-associated teleconnections lead to strong and widespread MHWs in the Northeast Pacific by June 2024. OAXs (Ω_a) are projected to be widespread by the middle of 2024

https://doi.org/10.1038/s41561-024-01593-0

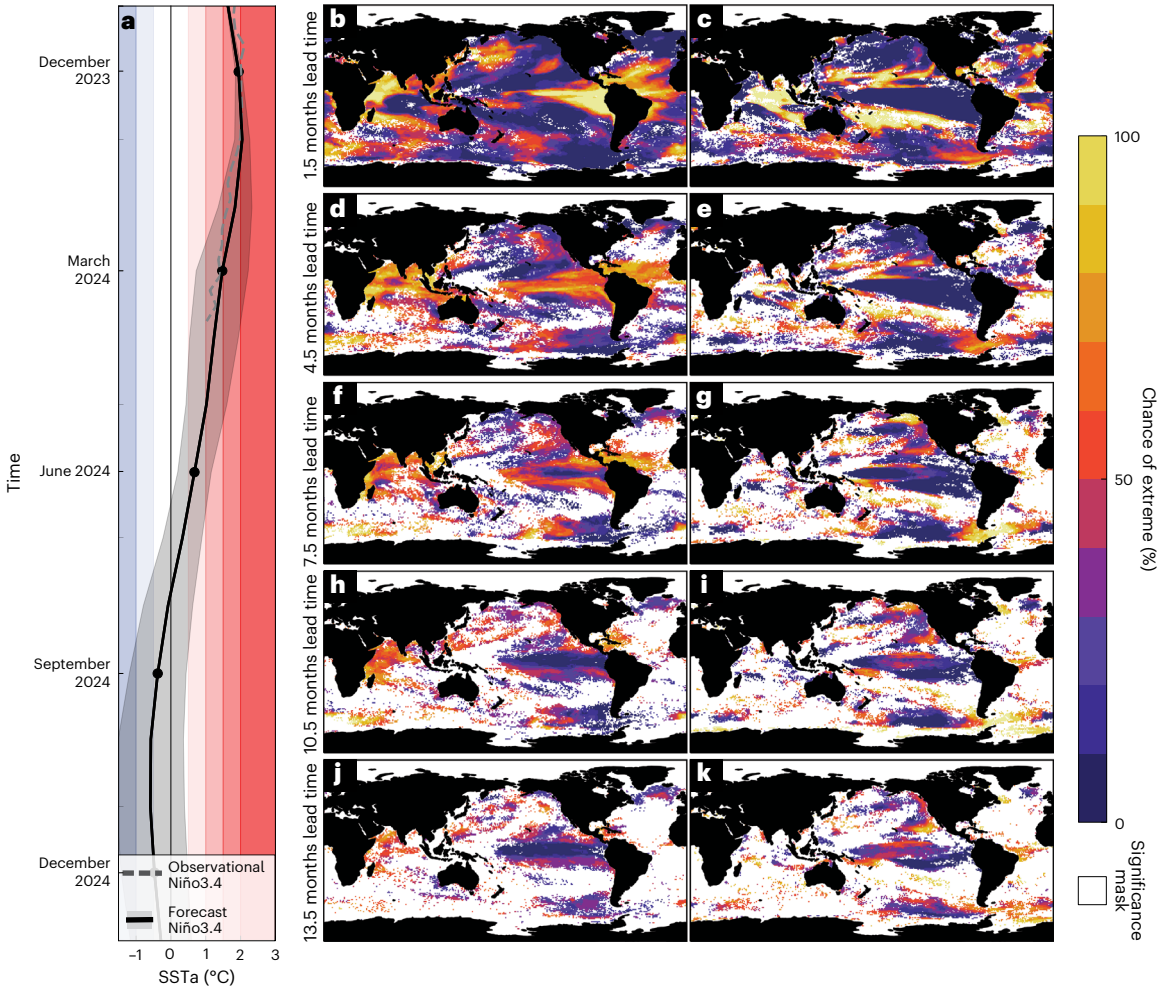

Fig. 4 | CESM SMYLE forecasts of Niño3.4, MHW and OAX initialized in November 2023. a, Niño3.4 SST anomaly from CESM SMYLE (solid black) with standard deviation (grey shading) and observations (dashed). **b**–**k**, Likelihood of MHWs as a percentage of model ensemble members at increasing lead time (**b**, **d**, **f**, **h** and **j**) and likelihood of OAX (Ω_a) as a percentage of model ensemble members at increasing lead time (**c**, **e**, **g**, **i** and **k**), masked by areas significantly skilful in the historical period at the given forecast lead time relative to 1,000 random forecasts at the 95% confidence interval.

(Fig. 4c,e,g,i,k). The initial stages of this El Niño event are associated with widespread OAX events (for example, in the Indian and subtropical Pacific), although not in the eastern tropical Pacific (probably connected to surface warming in the eastern tropical Pacific suppressing low Ω_a conditions[48]). By December 2024, we forecast extreme conditions in Ω_a in the Northeast Pacific and equatorial Atlantic. While we limit our forecast analysis to the 13 months following initialization in November 2023, a subsequent La Niña event would probably be associated with strong OAX events in the eastern Pacific (as in the historical record in Extended Data Fig. 6, which shows an example forecast generated during the 1999–2000 La Niña event with widespread OAX events in the eastern Pacific).

Managing marine systems in the coming decades will require improved and expanded forecasts that include marine stressors beyond temperature[49]. The forecasts displayed in Fig. 4 should encourage plans to expand existing operational forecasting systems (for example, at NOAA Physical Sciences Laboratory[50] and Mercator Ocean International[51]) to represent marine biogeochemistry, allowing for outlooks on extremes in key ecosystem stressors. Accurate forecasts of marine dynamics and extremes can better inform contemporary practices of marine managers, especially in a changing climate[8,52,53]. While our study does not make concrete policy recommendations, we hope that this work encourages the inclusion of biogeochemical and carbon cycle models in operational forecasts and seasonal outlooks that currently include only physical tracers. While OAXs are less well studied than MHWs, they are demonstrably predictable and have potentially dramatic ramifications for ecosystems. Future studies should focus on forecasting concurrent extremes, especially those that are dynamically favoured to co-occur (for example, MHW and OAX [H^+]), and examine underlying definitions of extreme events (for example, potentially using an absolute rather than statistical definition of an extreme). As operational forecasts of MHWs become more mainstream (as at the National Oceanic and Atmospheric Administration Physical Sciences Lab and Mercator Ocean International), the inclusion of biogeochemical extremes would help better inform the health of marine ecosystems.

Online content

Any methods, additional references, Nature Portfolio reporting summaries, source data, extended data, supplementary information, acknowledgements, peer review information; details of author contributions and competing interests; and statements of data and code availability are available at https://doi.org/10.1038/s41561-024-01593-0.

References

1. Doney, S. C., Fabry, V. J., Feely, R. A. & Kleypas, J. A. Ocean acidification: the other CO_2 problem. *Annu Rev. Mar. Sci.* **1**, 169–192 (2009).

2. Bopp, L. et al. Multiple stressors of ocean ecosystems in the 21st century: projections with CMIP5 models. *Biogeosciences* **10**, 6225–6245 (2013).
3. Kwiatkowski, L. & Orr, J. C. Diverging seasonal extremes for ocean acidification during the twenty-first century. *Nat. Clim. Chang.* **8**, 141–145 (2018).
4. Heinze, C. et al. Reviews and syntheses: abrupt ocean biogeochemical change under human-made climatic forcing—warming, acidification, and deoxygenation. Preprint at *Biogeosci. Discuss*. https://doi.org/10.5194/bg-2023-182 (2023).
5. Mogen, S. C. et al. Ocean biogeochemical signatures of the North Pacific Blob. *Geophys. Res. Lett.* https://doi.org/10.1029/2021GL096938 (2022).
6. Frölicher, T. L. & Laufkötter, C. Emerging risks from marine heat waves. *Nat. Commun.* **9**, 650 (2018).
7. Kohlman, C. et al. The 2019 marine heatwave at Ocean Station Papa: a multi-disciplinary assessment of ocean conditions and impacts on marine ecosystems. *J. Geophys. Res. Oceans* https://doi.org/10.1029/2023JC020167 (2024).
8. Jacox, M. G. et al. Global seasonal forecasts of marine heatwaves. *Nature* **604**, 486–490 (2022).
9. Hobday, A. J. et al. A hierarchical approach to defining marine heatwaves. *Prog. Oceanogr.* **141**, 227–238 (2016).
10. Holbrook, N. J. et al. A global assessment of marine heatwaves and their drivers. *Nat. Commun.* **10**, 2624 (2019).
11. Di Lorenzo, E. & Mantua, N. Multi-year persistence of the 2014/15 North Pacific marine heatwave. *Nat. Clim. Chang.* **6**, 1042–1047 (2016).
12. Amaya, D. J., Miller, A. J., Xie, S.-P. & Kosaka, Y. Physical drivers of the summer 2019 North Pacific marine heatwave. *Nat. Commun.* **11**, 1903 (2020).
13. Scannell, H. et al. Spatiotemporal evolution of marine heatwaves globally. Preprint at *ESS Open Archive* https://doi.org/10.22541/essoar.169008275.57053412/v1 (2023).
14. Guo, X. et al. Threat by marine heatwaves to adaptive large marine ecosystems in an eddy-resolving model. *Nat. Clim. Chang.* **12**, 179–186 (2022).
15. Wyatt, A. M., Resplandy, L. & Marchetti, A. Ecosystem impacts of marine heat waves in the northeast Pacific. *Biogeosciences* **19**, 5689–5705 (2022).
16. Rühmkorff, S. et al. Marine heatwaves and upwelling shape stress responses in a keystone predator. *Proc. R. Soc. B* **290**, 20222262 (2023).
17. Welch, H. et al. Impacts of marine heatwaves on top predator distributions are variable but predictable. *Nat. Commun.* **14**, 5188 (2023).
18. Smale, D. A. et al. Marine heatwaves threaten global biodiversity and the provision of ecosystem services. *Nat. Clim. Chang.* **9**, 306–312 (2019).
19. Fragkopoulou, E. et al. Marine biodiversity exposed to prolonged and intense subsurface heatwaves. *Nat. Clim. Chang.* https://doi.org/10.1038/s41558-023-01790-6 (2023).
20. Hauri, C. et al. Spatiotemporal variability and long-term trends of ocean acidification in the California Current System. *Biogeosciences* **10**, 193–216 (2013).
21. Hauri, C., Friedrich, T. & Timmermann, A. Abrupt onset and prolongation of aragonite undersaturation events in the Southern Ocean. *Nat. Clim. Chang.* **6**, 172–176 (2016).
22. Burger, F. A., John, J. G. & Frölicher, T. L. Increase in ocean acidity variability and extremes under increasing atmospheric CO_2. *Biogeosciences* **17**, 4633–4662 (2020).
23. Burger, F. A. & Frölicher, T. L. Drivers of surface ocean acidity extremes in an Earth system model. *Global Biogeochem. Cycles* **37**, e2023GB007785 (2023).
24. Desmet, F., Gruber, N., Köhn, E. E., Münnich, M. & Vogt, M. Tracking the space–time evolution of ocean acidification extremes in the California Current System and Northeast Pacific. *J. Geophys. Res. Oceans* https://doi.org/10.1029/2021JC018159 (2022).
25. Wong, J., Münnich, M. & Gruber, N. Column-compound extremes in the global ocean. AGU Adv. *AGU Adv.* **5**, e2023AV001059 (2024).
26. Mucci, A. The solubility of calcite and aragonite in seawater at various salinities, temperatures, and one atmosphere total pressure. *Am. J. Sci.* **283**, 780–799 (1983).
27. Ries, J. B., Cohen, A. L. & McCorkle, D. C. Marine calcifiers exhibit mixed responses to CO_2-induced ocean acidification. *Geology* **37**, 1131–1134 (2009).
28. Bednaršek, N. et al. Systematic review and meta-analysis toward synthesis of thresholds of ocean acidification impacts on calcifying pteropods and interactions with warming. *Front Mar. Sci.* **6**, 227 (2019).
29. Negrete-García, G., Lovenduski, N. S., Hauri, C., Krumhardt, K. M. & Lauvset, S. K. Sudden emergence of a shallow aragonite saturation horizon in the Southern Ocean. *Nat. Clim. Chang.* **9**, 313–317 (2019).
30. Bednaršek, N., Harvey, C. J., Kaplan, I. C., Feely, R. A. & Možina, J. Pteropods on the edge: cumulative effects of ocean acidification, warming, and deoxygenation. *Prog. Oceanogr.* **145**, 1–24 (2016).
31. Bednaršek, N. et al. El Niño-related thermal stress coupled with upwelling-related ocean acidification negatively impacts cellular to population-level responses in pteropods along the California Current System with implications for increased bioenergetic costs. *Front Mar. Sci.* **5**, 486 (2018).
32. Bednaršek, N. et al. Exposure history determines pteropod vulnerability to ocean acidification along the US West Coast. *Sci. Rep.* **7**, 4526 (2017).
33. Bednaršek, N. et al. Integrated assessment of ocean acidification risks to pteropods in the northern high latitudes: regional comparison of exposure, sensitivity and adaptive capacity. *Front Mar. Sci.* **8**, 671497 (2021).
34. Manno, C., Peck, V. L. & Tarling, G. A. Pteropod eggs released at high p_{CO_2} lack resilience to ocean acidification. *Sci. Rep.* **6**, 25752 (2016).
35. Stock, C. A. et al. Seasonal sea surface temperature anomaly prediction for coastal ecosystems. *Prog. Oceanogr.* **137**, 219–236 (2015).
36. Mogen, S. C. et al. Skillful multi-month predictions of ecosystem stressors in the surface and subsurface ocean. *Earths Future* **11**, e2023EF003605 (2023).
37. Brady, R. X., Lovenduski, N. S., Yeager, S. G., Long, M. C. & Lindsay, K. Skillful multiyear predictions of ocean acidification in the California Current System. *Nat. Commun.* **11**, 2166 (2020).
38. McAdam, R., Masina, S. & Gualdi, S. Seasonal forecasting of subsurface marine heatwaves. *Commun. Earth Environ.* **4**, 225 (2023).
39. Yeager, S. G. et al. The Seasonal-to-Multiyear Large Ensemble (SMYLE) prediction system using the Community Earth System Model version 2. *Geosci. Model Dev.* **15**, 6451–6493 (2022).
40. Jacox, M. G. et al. Seasonal-to-interannual prediction of North American coastal marine ecosystems: forecast methods, mechanisms of predictability, and priority developments. *Prog. Oceanogr.* **183**, 102307 (2020).
41. Capotondi, A., Sardeshmukh, P. D., Di Lorenzo, E., Subramanian, A. C. & Miller, A. J. Predictability of US West Coast ocean temperatures is not solely due to ENSO. *Sci. Rep.* **9**, 10993 (2019).
42. Capotondi, A., Newman, M., Xu, T. & Di Lorenzo, E. An optimal precursor of Northeast Pacific marine heatwaves and Central Pacific El Niño events. *Geophys. Res. Lett.* **49**, e2021GL097350 (2022).

43. Ren, X., Liu, W., Capotondi, A., Amaya, D. J. & Holbrook, N. J. The Pacific Decadal Oscillation modulated marine heatwaves in the Northeast Pacific during past decades. *Commun. Earth Environ.* **4**, 218 (2023).
44. Sarmiento, J. L. & Gruber, N. *Ocean Biogeochemical Dynamics* (Princeton Univ. Press, 2013); http://www.jstor.org/stable/10.2307/j.ctt3fgxqx
45. Lovenduski, N. S. et al. The potential impact of nuclear conflict on ocean acidification. *Geophys Res Lett.* **47**, e2019GL086246 (2020).
46. Reynolds, R. W. et al. Daily high-resolution-blended analyses for sea surface temperature. *J. Clim.* **20**, 5473–5496 (2007).
47. NOAA Earth System Research Laboratory. Niño3.4, https://stateoftheocean.osmc.noaa.gov/sur/pac/nino34.php (2024).
48. Lilly, L. E. et al. Biogeochemical anomalies at two Southern California Current System moorings during the 2014–2016 Warm Anomaly–El Niño sequence. *J. Geophys Res. Oceans* **124**, 6886–6903 (2019).
49. Mills, K. E. et al. in *Ocean Ecosystems and Marine Resources* (eds Crimmins, A. et al.) (US Global Change Research Program, 2023).
50. NOAA Physical Sciences Laboratory. Marine Heatwaves Forecast, https://psl.noaa.gov/marine-heatwaves/#forecasts (2024).
51. Mercator Ocean International. Marine Heatwave Bulletin, https://www.mercator-ocean.eu/en/category/mhw-bulletin/ (2024).
52. Siedlecki, S. A. et al. Experiments with seasonal forecasts of ocean conditions for the northern region of the California Current upwelling system. *Sci. Rep.* **6**, 27203 (2016).
53. Brodie, S. et al. Ecological forecasts for marine resource management during climate extremes. *Nat. Commun.* **14**, 7701 (2023).

[1]Department of Atmospheric and Oceanic Sciences and Institute of Arctic and Alpine Research, University of Colorado, Boulder, CO, USA. [2]NSF National Center for Atmospheric Research, Climate and Global Dynamics Lab, Boulder, CO, USA. [3]Cooperative Institute for Research in Environmental Sciences, University of Colorado, Boulder, CO, USA. [4]National Oceanic and Atmospheric Administration Physical Sciences Laboratory, Boulder, CO, USA. [5]National Oceanic and Atmospheric Administration Southwest Fisheries Science Center, Monterey, CA, USA. [6]Department of Earth, Environmental, and Planetary Sciences, Brown University, Providence, RI, USA. [7]Institute of Marine Sciences, University of California Santa Cruz, Monterey, CA, USA. ✉e-mail: samuel.mogen@colorado.edu

Methods

CESM SMYLE

CESM SMYLE was developed in the CESM2 framework and includes explicit rendering of marine biogeochemistry with the Marine Biogeochemistry Library, configured with three explicit phytoplankton functional groups (diatoms, diazotrophs and picophytoplankton), one implicit group (calcifiers), a single zooplankton type, multi-nutrient co-limitation (N, P, Si, Fe) and prognostic marine carbonate chemistry across 62 vertical model levels and nominal 1° horizontal resolution[54–57]. CESM SMYLE was initialized from the SMYLE FOSI reconstruction, an ocean–sea-ice-only simulation forced with the Japanese 55 year Reanalysis[58] momentum, heat and freshwater fluxes from 1958 to 2019 and atmospheric CO_2 concentrations. CESM SMYLE was initialized four times per year (1 February, 1 May, 1 August, 1 November) from 1970 to 2019 with an integration time of 2 years. A slight perturbation of surface air temperature is included at each initialization to generate 20 ensemble members. More detail on the CESM SMYLE hindcast can be found in refs. 36,39. Output utilized in this study is saved at monthly temporal resolution. Alongside the hindcast initializations of CESM SMYLE (1970–2019), we also analyse a CESM SMYLE forecast initialized in November 2023 from the SMYLE FOSI that was extended using near real-time updates to the JRA-55-based surface dataset for driving ocean–sea-ice models[58]. See Extended Data Fig. 7 for an example of two initializations of CESM SMYLE (November 2006 and November 2009) in the hindcast period.

Observational products

MHW and OAX events were identified in the observational record on the basis of OceanSODA-ETHZ, which interpolates surface ocean partial pressure of CO_2 (p_{CO_2}; from the Surface Ocean CO_2 Atlas)[59] and alkalinity (from the Global Ocean Data Analysis Project)[60] observations using machine-learning techniques[61] at nominal 1° horizontal resolution and monthly temporal resolution. Global alkalinity and p_{CO_2} estimates are then used to solve the full carbonate system using PyCO2SYS to generate estimates for all carbonate tracers[62]. SST is from Operational Sea Surface Temperature and Sea Ice Analysis[63,64]. OceanSODA-ETHZ includes historical data from 1982 to 2022, is well validated and has been used in previous studies on marine carbonate chemistry[65] and extremes[5].

Defining extremes

We calculate statistical extremes using the definition widely adopted in the literature[9,10,22]. Extended Data Fig. 8 displays the relative magnitude of statistical extremes compared with seasonal, interannual and multidecadal variability. While seasonal variability is prominent in the extratropical oceans, the magnitude of extremes can be as large, if not larger than, the other sources of variability in the tropics and northeast Pacific (Extended Data Fig. 8). We remove the long-term anthropogenic trend and the seasonal climatology for SST, Ω_a and $[H^+]$ at each grid cell in observations and CESM SMYLE as in ref. 8. We choose to remove long-term anthropogenic warming and acidification trends in our assessment of extreme events to account for shifting baselines in marine ecosystems as suggested by ref. 66. In observations, MHWs are defined by first removing seasonal climatologies and long-term warming trends (first-order polynomial). Then a rolling three-monthly threshold is created centred on the month of interest, and the 90th percentile threshold is calculated. In CESM SMYLE, a similar procedure was followed by first removing model climatology and long-term trends (along the dimension of year of initialization) from each ensemble member. Then a rolling three-lead-time (three monthly) threshold was calculated, centred on the lead time (month) of interest. Values above this threshold were again considered extreme. This methodology was repeated for $[H^+]$ (removing a second-order polynomial trend, extreme above the 90th percentile) and Ω_a (removing a second-order polynomial trend, extreme below the 10th percentile). We process the November 2023 SMYLE initialization in the same manner as for November-initialized hindcast. As noted, Ω_a is most detrimental to marine organisms when below saturation ($\Omega_a < 1$), but we choose to rely on a statistical definition of extremes following previous work[23,67]. The usefulness of statistical definitions of extremes may have a limit compared with a threshold based on an absolute value (for example, assuming organisms have limited adaptability outside of statistical thresholds, rather than an absolute stress threshold), but they prove useful when assessing skill across multiple forms of extremes across the global ocean as noted by ref. 68. See Extended Data Fig. 7 for an example of the appearance of OAX (Ω_a) in CESM SMYLE and SMYLE FOSI in the hindcast period.

Impacts of ENSO

Principal component analysis was completed for variables of interest (SST, Ω_a and $[H^+]$) from SMYLE FOSI over the hindcast period (1982–2019) in the tropical Pacific (30° S to 30° N, and 140° E to 280° E) by computing eigenvalues/eigenvectors of spatially weighted anomaly covariance matrices. The standardized first principal components of SST, Ω_a and $[H^+]$ were compared with a 5 month running mean of the Niño3.4 index (SST anomalies from 5° S to 5° N and 170° W to 120° W). The first principal components were then regressed onto SMYLE FOSI anomalies to illustrate the spatial patterns associated with the leading principal components (EOFs) for each tracer. Anomaly correlation coefficients were calculated for the first principal component of each variable of interest and the running Niño index, with significance estimated at the 95% confidence interval.

In an effort to disentangle the drivers of $[H^+]$ and Ω_a variability, the linear impact of temperature on $[H^+]$ was determined using the pyCO2SYS software[62] by varying temperature and holding all other inputs constant at their climatological mean values. Temperature effects are removed by calculating the $[H^+]$ variability driven by the thermal component ($[H^+]_t$) throughout the model historical record and subtracting that from $[H^+]$, leaving the nonthermal component ($[H^+]_{nt}$). Principal component analysis was then repeated for nonthermal values to determine the dominant modes of variability with the temperature effects removed.

To determine the impact of ENSO state at initialization on model forecast skill, we separate forecasts by those initialized during El Niño (Niño3.4 SSTa greater than 0.5 °C) and La Ninã (Niño3.4 SSTa less than −0.5 °C) and those initialized during neutral ENSO state (Niño3.4 SSTa between −0.5 °C and 0.5 °C). We then assess skill for these separate forecasts and take the difference in forecast skill at each lead time to determine the impact of ENSO state at initialization.

Drivers of Ω_a forecast skill

We analyse drivers of OAX (Ω_a) using the model definition of Ω_a:

$$\Omega_a \approx \frac{[CO_3^{2-}]}{[CO_3]_{saturation,aragonite}} \quad (1)$$

where $[CO_3]^{2-}$ and $[CO_3]^{2-}_{saturation,aragonite}$ are estimated at each model time step. Changes during extremes are driven by $[CO_3]^{2-}$ as $[CO_3]^{2-}_{saturation,aragonite}$ is largely a function of pressure. The expected changes in $[CO_3]^{2-}$ during extreme events are decomposed into contributions from temperature, salinity, DIC and alkalinity using relationships derived with pyCO2sys[62]. We take the difference between periods of extreme events and all times, indicating which are the most important terms in driving changes in Ω_a. We decompose the DIC response to extreme events using model output tendency terms, including total DIC tendency, air–sea CO_2 flux and biological flux. Circulation tendency is calculated as the residual:

$$DIC_{circulation,tendency} = DIC_{tendency} - Air\ Sea\ Flux_{tendency} - Biological_{tendency} \quad (2)$$

As with $[CO_3]^{2-}$, we take the difference between tendency terms during extreme events and all times.

Skill analysis

We combine all annual initializations for analysis of skill (relative to OceanSODA-ETHZ) and predictability (relative to SMYLE FOSI), as previous literature has found little impacts of initialization month on global ocean biogeochemical forecast skill (for example, ref. 36). Combining initializations further increased the number of forecasts being evaluated, increasing the statistical robustness of results. To assess forecast skill, we follow established methodologies for evaluating relatively infrequent climatic extremes: the SEDI skill score, forecast accuracy and Brier Skill Score. First, we classify each grid cell at each time into a 2 × 2 contingency table: true positive (extreme event is forecast and does appear in observations), false positive (extreme event is forecast but does not appear), false negative (extreme event is not forecast but does appear) and true negatives (extreme event is not forecast and does not appear). Using this contingency table, we then calculate SEDI and forecast accuracy. We also calculated the Brier Skill Score on the basis of the average of the binary forecasts from all ensemble members at a given time.

We follow ref. 8 in using SEDI as our primary skill metric. As noted in their work, it does not trend towards a meaningless limit as rarity increases, it is base-rate independent (not influenced by changes in event frequency), and it is equitable (random forecasts give an expected value of zero, or no skill). SEDI scores of greater than zero indicate skill better than random chance, while skill of less than zero indicates worse than random chance of an event being forecast correctly[8,69,70]:

$$\mathrm{SEDI} = \frac{\log F - \log H - \log(1-F) + \log(1-H)}{\log F + \log H + \log(1-F) + \log(1-H)} \quad (3)$$

where H is the hit rate (rate of true positives to total observed events) and F is the false alarm rate (rate of false positives to total observed nonevents).

Significance of SEDI forecast skill is quantified using a Monte Carlo simulation with bootstrapping. For a given grid cell, we randomly sample (with replacement) each SMYLE forecast to generate random forecasts; skill is then calculated for random forecasts. This process is repeated 1,000 times to generate a distribution of random forecasts. We then calculate the 95% confidence interval for scores of the random forecast at each grid cell. Skill scores are considered significant if the forecast exceeds the 97.5th percentile of random forecast skill distribution.

We use the contingency table to calculate forecast accuracy, which is simply the fraction of correctly forecast events[8]:

$$\mathrm{FA} = \frac{\text{true positives} + \text{true negatives}}{N} \quad (4)$$

where N is the total number of forecasts being evaluated. For events that occur 10% of the time (as in this study for all metrics), the forecast accuracy for a random forecast is calculated as 0.82.

We also calculate the Brier Skill Score (BSS). First, the Brier Score (BrS) estimates the mean square error of the probabilistic forecast:

$$\mathrm{BrS} = \frac{1}{N}\sum_{i=1}^{N}(f_i - o_i)^2 \quad (5)$$

where N is the number of forecasts evaluated, f_i is the forecast probability from all ensemble members, o_i is the observed probability (zero or one). The BrS is then normalized relative to a reference forecast where events have a 10% chance of occurring:

$$\mathrm{BSS} = 1 - \frac{\mathrm{BrS}}{\mathrm{BrS}_{\mathrm{ref}}} \quad (6)$$

The resulting BSS ranges from one (perfect) to negative infinity, with zero indicating skill no better than random chance.

Data availability

The CESM Seasonal to Multiyear Large Ensemble and SMYLE FOSI are available at https://doi.org/10.26024/pwma-re41 (ref. 39). OceanSODA-ETHZ can be accessed at https://doi.org/10.25921/m5wx-ja34 (ref. 61).

Code availability

All figures were generated with the open-source software Python. Code used in processing and analysing CESM SMYLE output relative to SMYLE FOSI and OceanSODA-ETHZ can be found at https://doi.org/10.5281/zenodo.12103992 (ref. 71).

References

54. Moore, J. K., Doney, S. C., Kleypas, J. A., Glover, D. M. & Fung, I. Y. An intermediate complexity marine ecosystem model for the global domain. *Deep Sea Res. 2* **49**, 403–462 (2001).
55. Moore, J. K., Doney, S. C. & Lindsay, K. Upper ocean ecosystem dynamics and iron cycling in a global three-dimensional model. *Global Biogeochem. Cycles* **18**, GB4028 (2004).
56. Moore, J. K., Lindsay, K., Doney, S. C., Long, M. C. & Misumi, K. Marine ecosystem dynamics and biogeochemical cycling in the Community Earth System Model [CESM1(BGC)]: comparison of the 1990s with the 2090s under the RCP4.5 and RCP8.5 scenarios. *J. Clim.* **26**, 9291–9312 (2013).
57. Long, M. C. et al. Simulations with the Marine Biogeochemistry Library (MARBL). *J. Adv. Model. Earth Syst.* https://doi.org/10.1029/2021MS002647 (2021).
58. Tsujino, H. et al. JRA-55 based surface dataset for driving ocean–sea-ice models (JRA55-do). *Ocean Model.* **130**, 79–139 (2018).
59. Bakker, D. C. E. et al. A multi-decade record of high-quality fCO_2 data in version 3 of the Surface Ocean CO_2 Atlas (SOCAT). *Earth Syst. Sci. Data* **8**, 383–413 (2016).
60. Olsen, A. et al. GLODAPv2.2019—an update of GLODAPv2. *Earth Syst. Sci. Data* **11**, 1437–1461 (2019).
61. Gregor, L. & Gruber, N. OceanSODA-ETHZ: a global gridded data set of the surface ocean carbonate system for seasonal to decadal studies of ocean acidification. *Earth Syst. Sci. Data* **13**, 777–808 (2021).
62. Humphreys, M. P., Lewis, E. R., Sharp, J. D. & Pierrot, D. PyCO2SYS v1.7: marine carbonate system calculations in Python. *Geosci. Model Dev.* https://doi.org/10.5194/gmd-2021-159 (2022).
63. Good, S., Embury, O., Bulgin, C. & Mittaz, J. *ESA Sea Surface Temperature Climate Change Initiative (SST_cci): Level 4 Analysis Climate Data Record* Version 2.0 (CEDA, 2019); https://catalogue.ceda.ac.uk/uuid/aced40d7cb964f23a0fd3e85772f2d48
64. Good, S. et al. The current configuration of the OSTIA system for operational production of foundation sea surface temperature and ice concentration analyses. *Remote Sens.* **12**, 720 (2020).
65. Ma, D., Gregor, L. & Gruber, N. Four decades of trends and drivers of global surface ocean acidification. *Global Biogeochem. Cycles* **37**, e2023GB007765 (2023).
66. Amaya, D. J. et al. Marine heatwaves need clear definitions so coastal communities can adapt. *Nature* **616**, 29–32 (2023).
67. Hauri, C. et al. More than marine heatwaves: a new regime of heat, acidity, and low oxygen compound extreme events in the Gulf of Alaska. *AGU Adv.* **5**, e2023AV001039 (2024).
68. Gruber, N., Boyd, P. W., Frölicher, T. L. & Vogt, M. Biogeochemical extremes and compound events in the ocean. *Nature* **600**, 395–407 (2021).
69. Marshall, A. G. et al. Intra-seasonal drivers of extreme heat over Australia in observations and POAMA-2. *Clim. Dyn.* **43**, 1915–1937 (2014).

70. Ferro, C. A. T. & Stephenson, D. B. Extremal dependence indices: improved verification measures for deterministic forecasts of rare binary events. *Weather Forecast.* **26**, 699–713 (2011).
71. Mogen, S. Marine extreme forecasting in CESM SMYLE (multi-month forecasts of marine heatwaves and ocean acidification extremes). *Zenodo* https://doi.org/10.5281/zenodo.12103992 (2024).

Acknowledgements

S.M. and N.S.L. were supported by the National Science Foundation (OCE 1752724) and the National Oceanic and Atmospheric Administration (NA20OAR4310405). M.P.B. was supported by the National Oceanic and Atmospheric Administration (NA20OAR4310405). S.J.Y. and N.R. acknowledge support from the Regional and Global Model Analysis (RGMA) component of the Earth and Environmental System Modeling Program of the US Department of Energy's Office of Biological and Environmental Research (BER) under award number DE-SC0022070. W.K. and S.J.Y. acknowledge the support of NOAA Climate Program Office's CVP programme under grant no. NA20OAR4310408. A.C. was supported by the NOAA Climate Program Office's MAPP programme, DOE Award no. DE-SC0023228, and NASA Physical Oceanography grant no. 80NSSC21K0556. This work also was supported by the National Center for Atmospheric Research, which is a major facility sponsored by the National Science Foundation (NSF) under Cooperative Agreement no. 1852977. We thank the National Center for Atmospheric Research Earth System Working Group for their development of invaluable software tools used in processing CESM SMYLE: https://github.com/CESM-ESPWG/ESP-Lab. We are grateful for helpful feedback from D. Amaya.

Author contributions

S.M. and N.S.L. designed the study. S.M. performed the analysis. All authors contributed to interpretation of the results. S.M. and N.S.L. wrote the manuscript with input from all authors.

Competing interests

The authors declare no competing interests.

Additional information

Extended data is available for this paper at https://doi.org/10.1038/s41561-024-01593-0.

Correspondence and requests for materials should be addressed to Samuel C. Mogen.

Peer review information *Nature Geoscience* thanks Filippa Fransner, James Orr and the other, anonymous, reviewer(s) for their contribution to the peer review of this work. Primary Handling Editor: James Super, in collaboration with the *Nature Geoscience* team.

https://doi.org/10.1038/s41561-024-01593-0

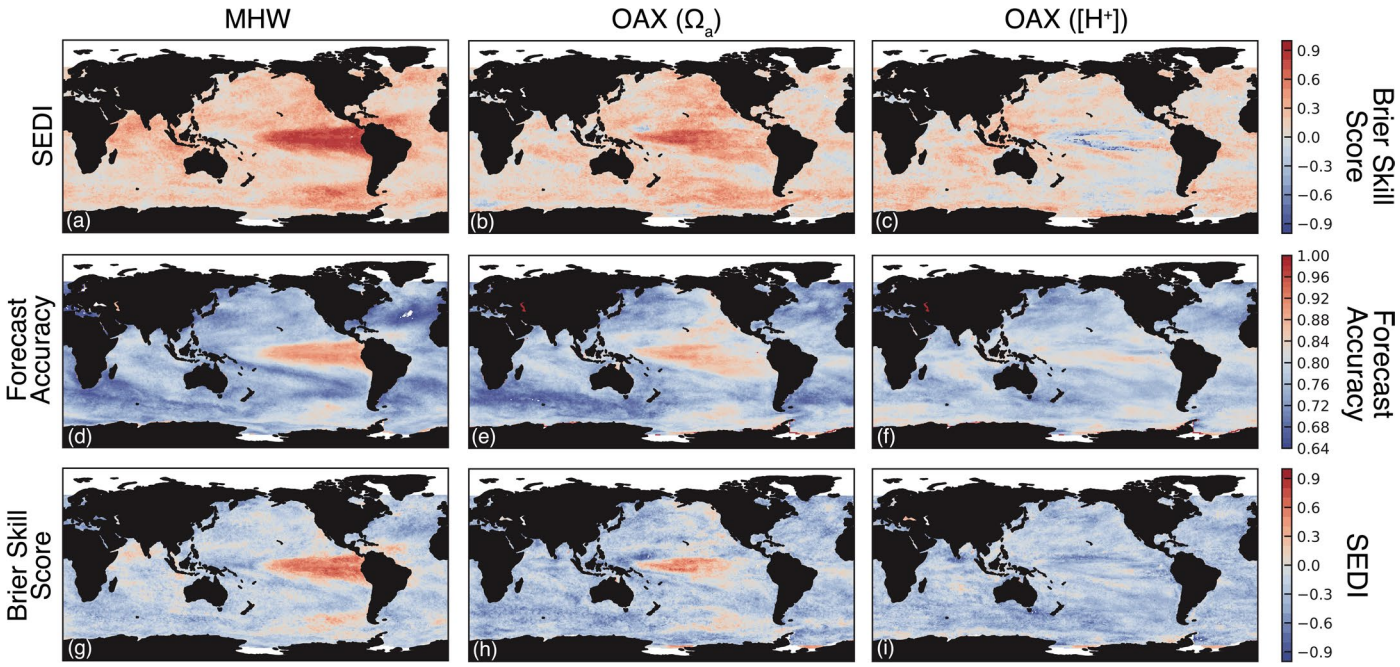

Extended Data Fig. 1 | Different skill metrics (SEDI, Forecast Accuracy, Brier Skill Score) at lead-time 3.5 months. Forecast skill calculated by three different metrics at lead-time 3.5 months. SEDI (as in Fig. 1) (row 1; **a**,**b**,**c**), Forecast Accuracy (row 2; **d**,**e**,**f**), and Brier Skill Score (BSS) (row 3: **g**,**h**,**i**) for marine heatwaves (column 1), ocean acidification extremes (Ω_a), and ocean acidification extremes ([H^+]).

https://doi.org/10.1038/s41561-024-01593-0

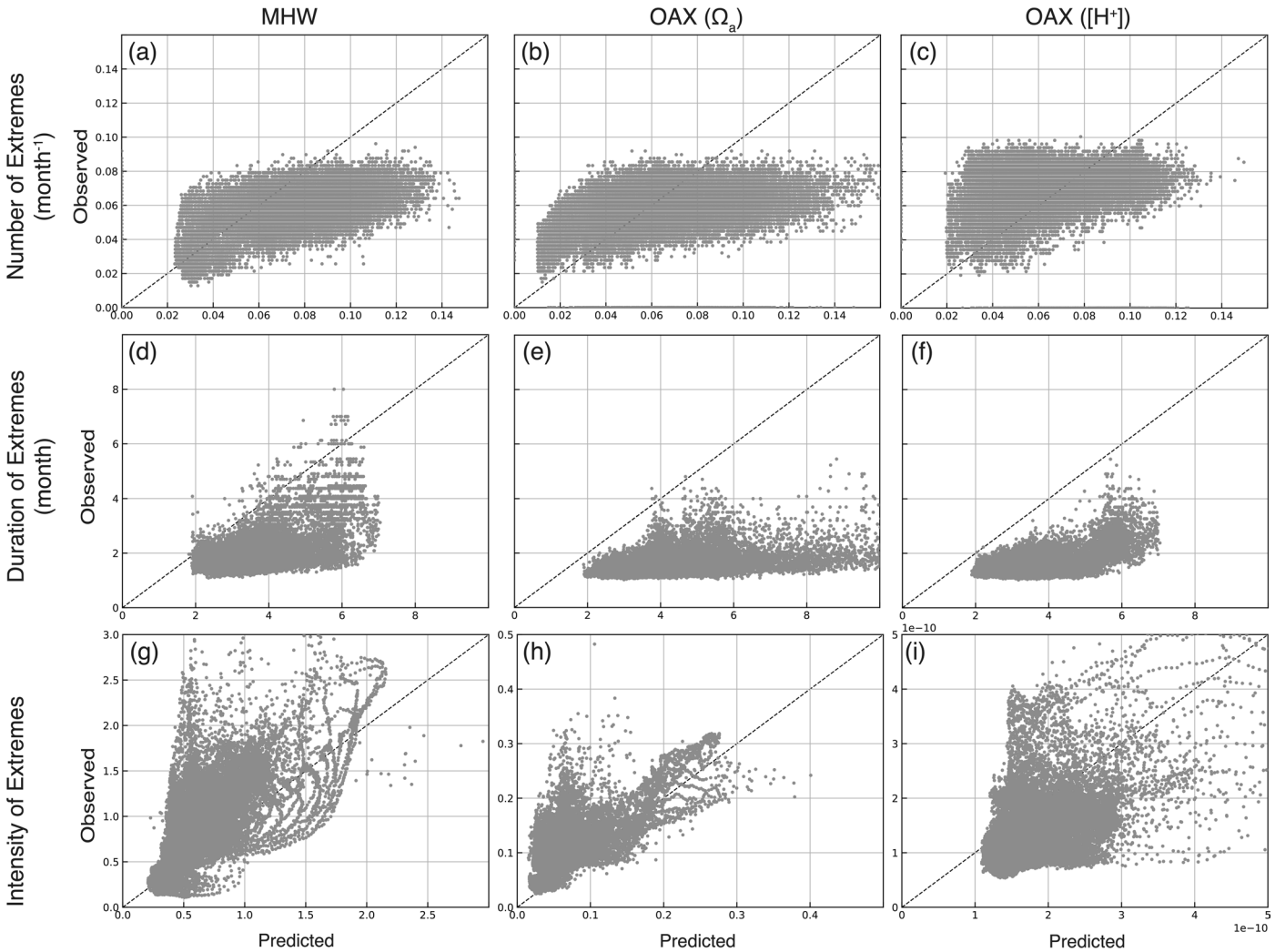

Extended Data Fig. 2 | Number, duration, and intensity of extremes in CESM SMYLE and observations. Number per month (row 1; **a**,**b**,**c**), duration (row 2; **d**,**e**,**f**), and intensity (row 3; **g**,**h**,**i**) of the average extreme event in observations and CESM SMYLE for marine heatwaves (column 1), ocean acidification extremes (Ω_a) (column 2), and ocean acidification extremes ($[H^+]$) (column 3) at each location.

https://doi.org/10.1038/s41561-024-01593-0

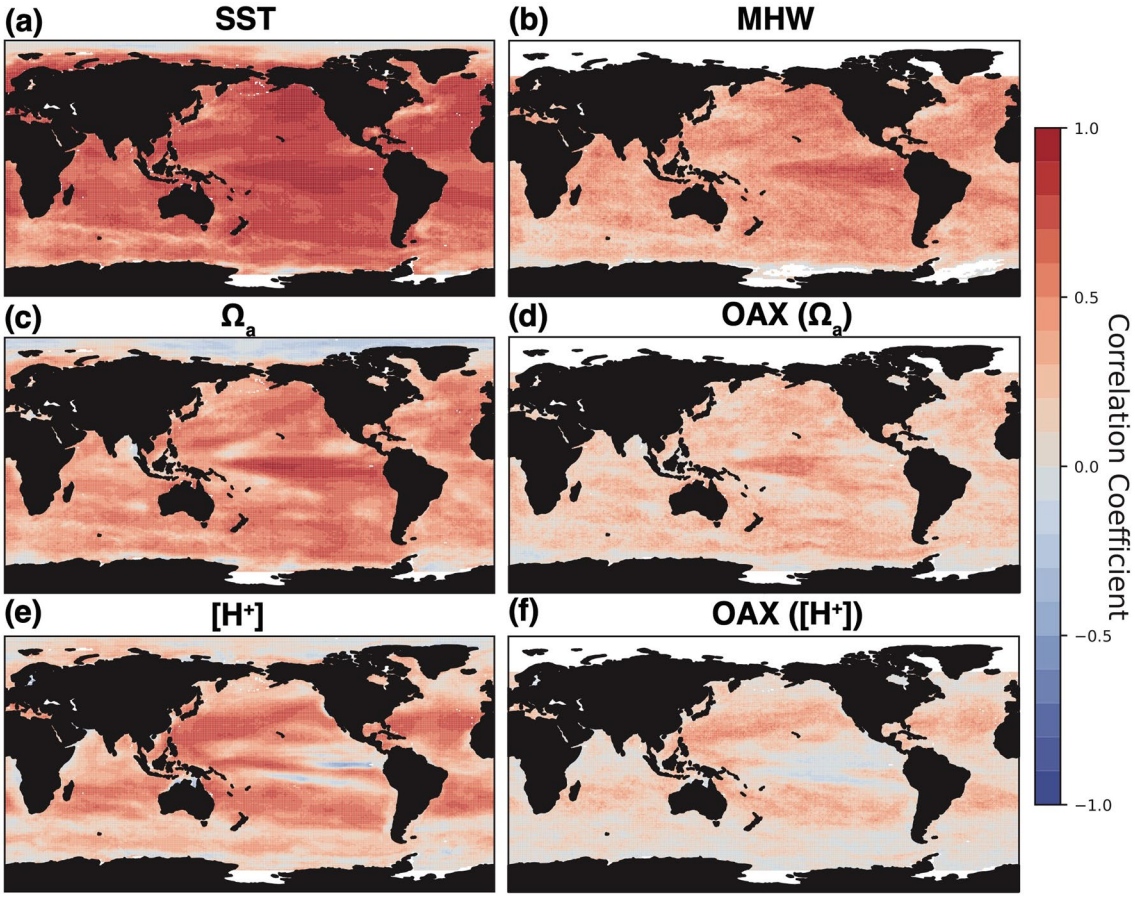

Extended Data Fig. 3 | Correlation between historically observed and modelled variability and extremes. Correlation coefficient between historical (column 1) variability of (**a**) sea surface temperature, (**c**) Ω_a, (**e**) [H^+] and (column 2) extremes (**b**) marine heatwaves, (**d**) ocean acidification extremes (Ω_a),(**f**) ocean acidification extremes ([H^+]) in SMYLE FOSI and observations (OceanSODA-ETHZ). Higher correlation coefficients indicate more similar historical variability or extreme events.

https://doi.org/10.1038/s41561-024-01593-0

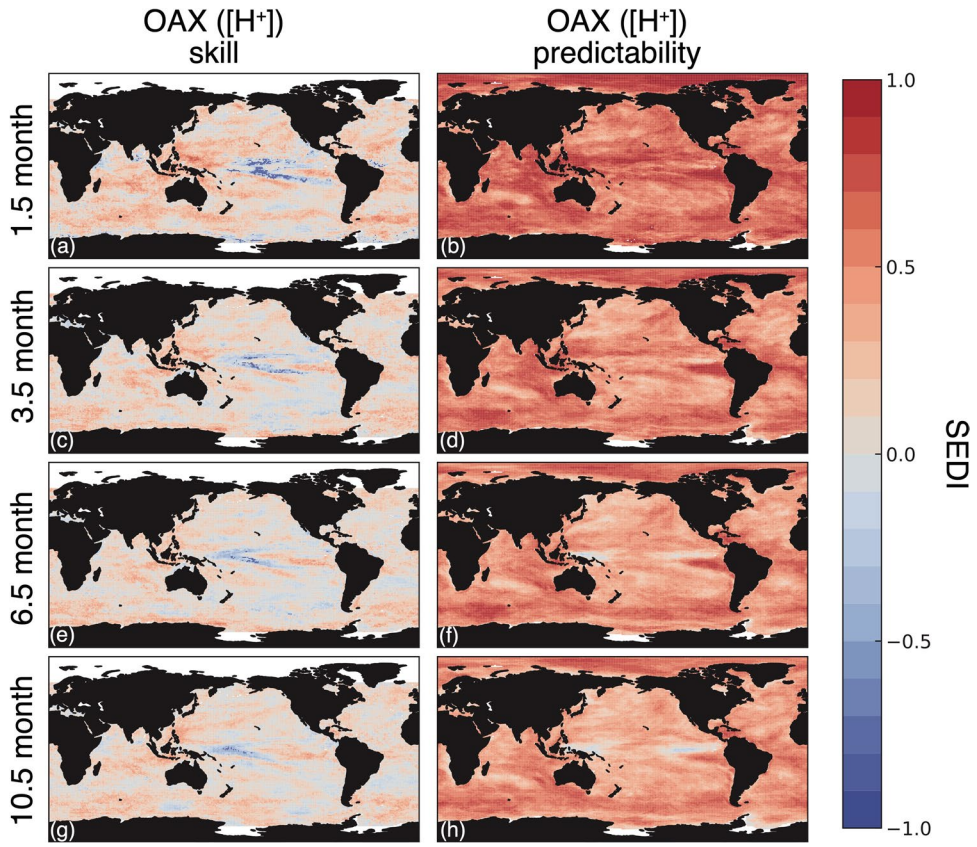

Extended Data Fig. 4 | Model skill (CESM SMYLE relative to observations) and model predictability (CESM SMYLE relative to SMYLE FOSI). Comparison of (column 1) model skill (CESM SMYLE relative to observations) and (column 2) model predictability (CESM SMYLE relative to SMYLE FOSI) for 20 ensemble members from CESM SMYLE at 1.5 (**a**-**b**), 3.5 (**c**-**d**), 6.5 (**e**-**f**), and 10.5 month lead-time (**g**-**h**). Skill scores range from -1 to 1, with SEDI score close to -1 being unskillful, SEDI score of 0 being no better than random forecasts, and SEDI score of 1 being perfect skill.

https://doi.org/10.1038/s41561-024-01593-0

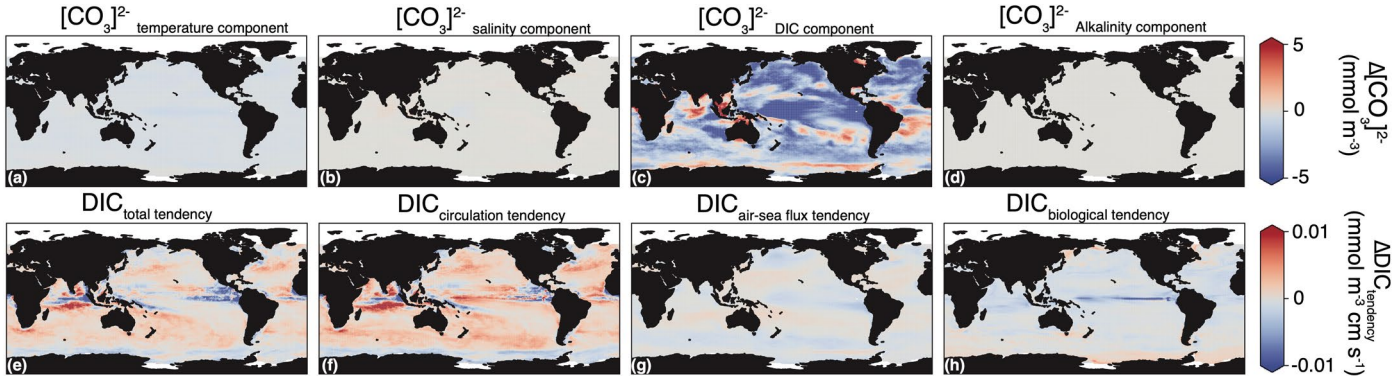

Extended Data Fig. 5 | Decomposition and drivers of extremes in aragonite saturation state. Decomposition of Ω_a to determine drivers of extreme events. (row 1) Decomposition of $[CO_3]^{2-}$ into drivers of changes during extremes relative to all times, including effects of (**a**) temperature, (**b**) salinity, (**c**) DIC, (**d**) Alkalinity. (row 2) Changes to tendency terms of DIC during extremes relative to all times, including: (**e**) total DIC tendency, (**f**) circulation tendency, (**g**) air-sea CO_2 flux tendency, and (**h**) biological tendency.

https://doi.org/10.1038/s41561-024-01593-0

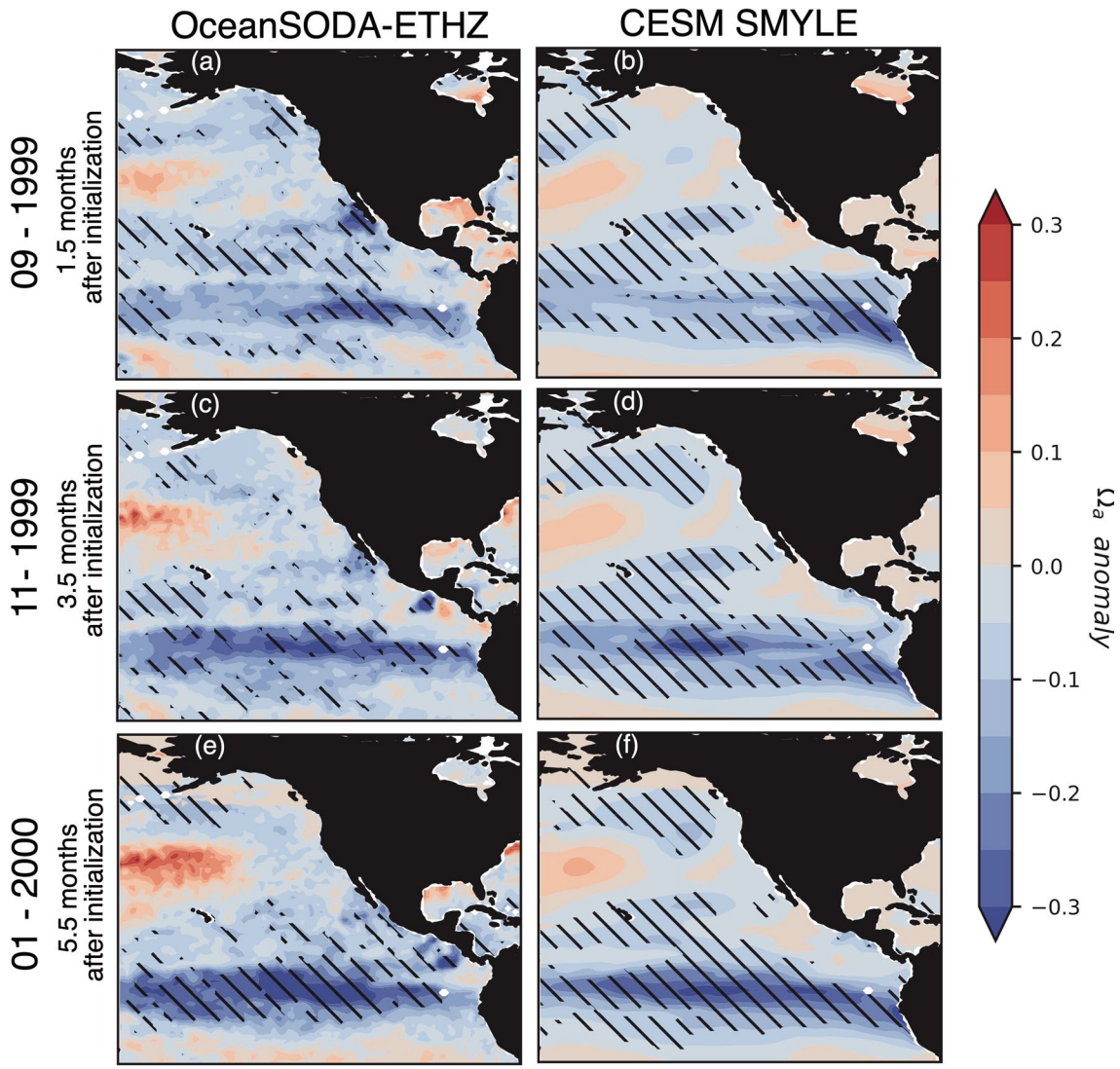

Extended Data Fig. 6 | Example forecast of aragonite saturation state extreme events from the 1999 La Niña. Forecasts of Ω_a initialized during the August 1999 La Niña event. Anomalies (color) and extremes (hatching) in (column 1) from an interpolated observational product (OceanSODA-ETHZ), and (column 2) CESM SMYLE forecasts (**a**,**b**) 1.5, (**c**,**d**) 3.5, and (**e**,**f**) 5.5 months after initialization. Extreme events are defined in observations (below the 10th percentile) and in CESM SMYLE (below the 10th percentile in a minimum of 50% of ensemble members).

https://doi.org/10.1038/s41561-024-01593-0

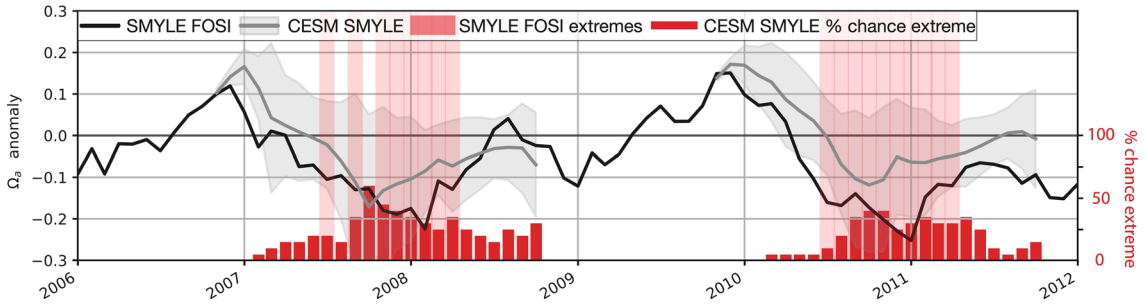

Extended Data Fig. 7 | Example forecast of aragonite saturation state extremes in the tropical Pacific from 2004-2012. Example timeseries of Ω_a anomalies in the central tropical Pacific (0.5°N, 138.5°W) for (black) SMYLE FOSI and (grey) two November CESM SMYLE initializations (2006a and 2009; with ensemble spread represented) from 2006-2012. Occurrence of extreme events are indicated for (red lines) SMYLE FOSI and (bar plot) CESM SMYLE (as a percentage of ensemble members).

https://doi.org/10.1038/s41561-024-01593-0

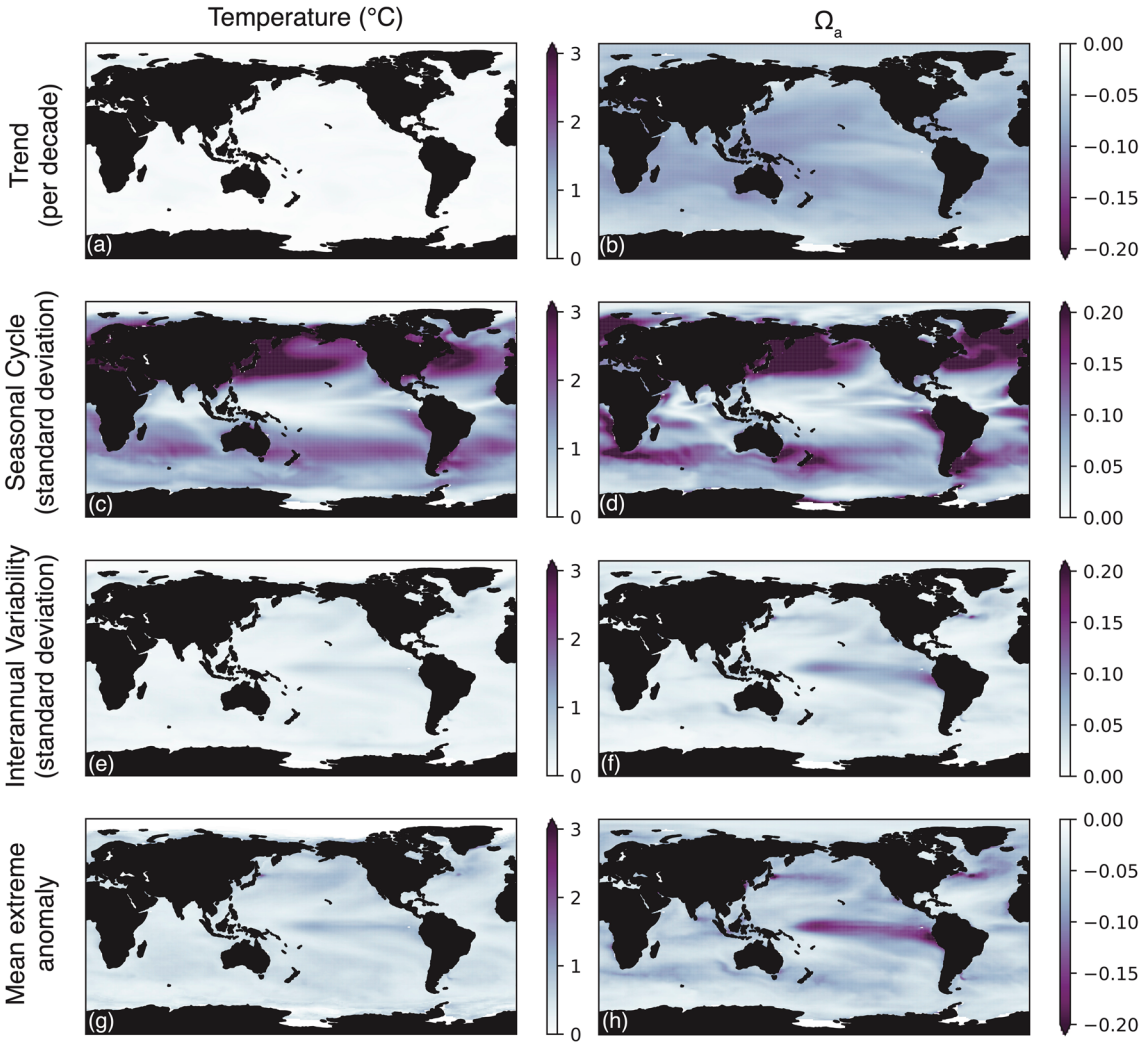

Extended Data Fig. 8 | Magnitude of variability associated with trend (per decade), climatology, interannual variability, and extreme event anomaly for aragonite saturation state. Relative magnitude of anomalies associated with (row 1; **a**,**b**) trend (per decade), (row 2; **c**,**d**) seasonal climatology, (row 3; **e**,**f**) interannual variability, and (row 4; **g**,**h**) mean strength of anomaly to generate extreme event for temperature and Ω_a.